

7N-34  
198529  
P-24

# TECHNICAL NOTE

D-265

EXPERIMENTAL RESULTS OF A HEAT-TRANSFER STUDY

FROM A FULL-SCALE PEBBLE-BED HEATER

By Richard B. Lancashire, Erwin A. Lezberg, and James F. Morris

Lewis Research Center  
Cleveland, Ohio

NATIONAL AERONAUTICS AND SPACE ADMINISTRATION

WASHINGTON

March 1960

(NASA-TN-D-265) EXPERIMENTAL RESULTS OF A  
HEAT-TRANSFER STUDY FROM A FULL-SCALE  
PEBBLE-BED HEATER (NASA. Lewis Research  
Center) 24 p

N89-70760

Unclas  
00/34 0198529

NATIONAL AERONAUTICS AND SPACE ADMINISTRATION

---

TECHNICAL NOTE D-265

---

EXPERIMENTAL RESULTS OF A HEAT-TRANSFER STUDY

FROM A FULL-SCALE PEBBLE-BED HEATER

By Richard B. Lancashire, Erwin A. Lezberg  
and James F. Morris

SUMMARY

A regenerative pebble-bed heat exchanger has been built in order to produce large quantities of high-temperature air for use in the experimental evaluation of hypersonic flight problems. During the initial operation of this facility, a program was carried out to obtain data concerning heat transfer in a large packed bed of spheres.

A detailed description is given of the facility design, operation, and instrumentation. The heat-transfer analysis, similar to that used by other investigators, is also presented. Samples of data obtained are shown with respect to their use in the analysis. Results of this work as compared with other investigators are presented in the conventional Stanton, Prandtl, and Reynolds numbers relation.

INTRODUCTION

The experimental evaluation of hypersonic flight problems requires the production of large quantities of high-temperature air. At temperatures above 2500° R, conventional heat exchangers have exceeded their material limits so that other heating methods must be used.

One such method is the use of the regenerative pebble-bed heat exchanger, utilizing high-temperature refractories (refs. 1, 2, and 3). The design of such a heat exchanger requires the use of reliable heat-transfer coefficients for a packed bed. A considerable amount of experimental data is available on the subject, but it spreads over two orders of magnitude at any one Reynolds number value.

The experimental work described in this report was performed on a full-scale pebble bed, 10.4 feet in length and 4 feet in diameter. The facility is used at the Lewis Research Center for testing air-breathing engine components. The purpose of this work was to obtain heat-transfer

data during the initial operation of the facility as a guide to the design of similar equipment. The exchanger was designed with a conservative estimate of the heat-transfer coefficient (ref. 4). Temperatures throughout the packing were measured continuously so that point values of the coefficient might be obtained.

# SYMBOLS

C	heat capacity of bed material, Btu/(°F)(cu ft packing)
$c_p$	specific heat of air, Btu/(lb)(°F)
d	average diameter of a bed particle, ft
G	mass velocity, lb air/(hr)(sq ft bed cross section)
h	heat-transfer coefficient, Btu/(hr)(°F)(sq ft pebble surface area)
Pr	Prandtl number
Re	Reynolds number, $Gd/\mu$
St	Stanton number, $h/Gc_p$
s	ratio of surface area of bed material to total volume of bed, 1/ft
$T_i$	blowdown air temperature at $x = 0$ , °R
t	bed temperature, °R
$t_0$	bed temperature at $\tau = 0$ , °R
x	distance from bottom of bed, ft
$\delta$	dimensionless bed temperature, $(t - T_i)/(t_0 - T_i)$
$\eta$	dimensionless time, $sh\tau/C$
$\mu$	viscosity of air, lb/(ft)(hr)
$\xi$	dimensionless distance, $shx/Gc_p$
$\tau$	time from beginning of blowdown, hr

## FACILITY

A schematic drawing of the facility is shown in figure 1. The bed is packed with 3/8-inch-diameter alumina balls and has 2-foot-thick walls made of high-temperature refractory and insulating brick to minimize the heat losses. The heater is designed to operate at a maximum temperature of 3500° R and a nominal pressure of 50 pounds per square inch absolute, with a maximum airflow of 10 pounds per second.

The bed is heated by burning gasoline and passing the combustion products down through the bed to an atmospheric exhaust. Heating is accomplished in two stages: The first uses a small banking burner located at the top flange (fig. 2). The banking burner is operated continuously except during blowdown. When the bed is hot, approximately 2200° R in the upper portion, long heating periods with the main burner are eliminated, and spalling of the refractory is kept to a minimum. The second-stage burner is also shown in figure 2. Fuel and combustion air are introduced into the annulus between the brick work and a water-cooled shroud. Ignition is provided by the banking burner and the hot refractory. The main burner is used to heat the upper portion of the bed to temperatures up to 3500° R. Transition to the blowdown part of the cycle is accomplished by actuating a three-way proportioning valve, which diverts air from the main burner to the bottom of the bed. The air, after passing through the heated bed and the test section, is quenched by water sprays and ducted to the laboratory exhaust system.

## INSTRUMENTATION

Thermocouples were fabricated from 20-gage Chromel-Alumel wires, and the junctions were cast in the center of 1/2-inch-diameter by 1/2-inch-long alumina cylinders. The lead wires were swaged into 1/16-inch Inconel protection tubes with magnesia insulation. Thermocouple locations in the bed are shown in figure 1. The thermocouples were wired in place before the bed was filled, and the lead wires were brought out through the bottom of the tank. The time lag due to measuring the temperature at the center of a cylinder rather than at the surface of a ball was estimated and indicated that the maximum error in measurement would be approximately 20° F.

During the process of cycling the bed, a number of the thermocouples failed or exhibited intermittent failure (open or partially open circuit). This type of failure appeared to be related to the attack of the Alumel wire by impurities in the magnesium oxide swaging material as indicated in reference 5.

Bed thermocouples were read at the rate of 20 per second using an automatic voltage digitizer, recorded, and processed by the laboratory

automatic data reduction system (ref. 6). The thermocouples were paralleled to a 40-channel oscilloscope, which was used as a visual check of the bed temperature profiles.

The hot air temperature was measured during blowdown with a platinum - platinum-rhodium aspirated thermocouple probe. The probe, as described in reference 7, has a support tube which is water-cooled with the exception of the platinum tip. The temperature was recorded on a strip chart recorder.

Pressure drop across the bed was measured with static taps at the air inlets to the top and bottom of the bed. Air was metered through a standard ASME orifice.

#### HEAT-TRANSFER ANALYSIS

The heat-transfer analysis used in this article is a variation of that used by Johnson (ref. 8). This analysis is based on the original analysis of nonsteady heat transfer in porous media by Schumann (ref. 9). The assumptions made in this analysis are as follows:

(1) The thermal diffusivity of the balls is considered very large. Thus, the only resistance to heat transfer between a ball and the fluid is judged to be in the film.

(2) Conduction in the radial direction of the bed is considered to be infinite and that in the direction of flow to be negligible.

(3) Conduction within the fluid is negligible.

(4) The fluid is considered to have a uniform velocity across the bed.

In accordance with Johnson, the following group of dimensionless parameters is used herein:

$$\text{Dimensionless length:} \quad \xi = shx/Gc_p \quad (1)$$

$$\text{Dimensionless time:} \quad \eta = sh\pi/C \quad (2)$$

$$\text{Dimensionless bed temperature:} \quad \delta = (t - T_i)/(t_0 - T_i) \quad (3)$$

Table I of reference 8 lists the dimensionless bed temperature  $\delta$  for various values of  $\eta$  and  $\xi$ . This table was prepared using the solutions of the differential equations of heat transfer for a regenerator. With these published data  $\delta$  was plotted as a function of  $\eta$  for

constant  $\xi$  values and against  $\xi$  for constant  $\eta$  values. The slopes of these curves yielded  $(\partial\delta/\partial\eta)_{\xi}$  and  $(\partial\delta/\partial\xi)_{\eta}$ . These are given in terms of their equivalent forms, which are easily related to measurable quantities:

$$\left(\frac{\partial\delta}{\partial\eta}\right)_{\xi} \equiv \left(\frac{\frac{\partial t}{t_0 - T_i}}{\frac{\text{sh}}{C} \frac{\partial \tau}{\partial x}}\right) = \frac{C}{\text{sh}(t_0 - T_i)} \left(\frac{\partial t}{\partial \tau}\right)_x \quad (4)$$

$$\left(\frac{\partial\delta}{\partial\xi}\right)_{\eta} \equiv \left(\frac{\frac{\partial t}{t_0 - T_i}}{\frac{\text{sh}}{Gc_p} \frac{\partial x}{\partial \tau}}\right) = \frac{Gc_p}{\text{sh}(t_0 - T_i)} \left(\frac{\partial t}{\partial x}\right)_{\tau} \quad (5)$$

Since the temperature  $t_0$  is not constant, another form of the temperature, considering its variation, must be used. Therefore, by substituting

$$t_0 = \frac{t - T_i}{\delta} + T_i \quad (3a)$$

equations (4) and (5) become

$$\frac{1}{\delta} \left(\frac{\partial\delta}{\partial\eta}\right)_{\xi} \equiv \frac{C}{\text{sh}(t - T_i)} \left(\frac{\partial t}{\partial \tau}\right)_x \quad (6)$$

and

$$\frac{1}{\delta} \left(\frac{\partial\delta}{\partial\xi}\right)_{\eta} \equiv \frac{Gc_p}{\text{sh}(t - T_i)} \left(\frac{\partial t}{\partial x}\right)_{\tau} \quad (7)$$

With the theoretical data of reference 8 and the slopes obtained from that data, the left sides of equations (6) and (7) have been plotted against their respective independent variables for various values of the constant parameters. These plots were made using logarithmic scales and are shown in figure 3.

By multiplying both sides of equations (6) and (7) by the heat-transfer coefficient  $h$ , these two equations become

$$\frac{h}{\delta} \left(\frac{\partial\delta}{\partial\eta}\right)_{\xi} \equiv \frac{C}{s(t - T_i)} \left(\frac{\partial t}{\partial \tau}\right)_x \quad (8)$$

$$\frac{h}{\delta} \left( \frac{\partial \delta}{\partial \xi} \right)_{\eta} \equiv \frac{G c_p}{s(t - T_i)} \left( \frac{\partial t}{\partial x} \right)_{\tau} \quad (9)$$

The right side of each equation was easily obtained from experimental data. The heat capacity of the bed material  $C$  was given by its manufacturer as 31.8 Btu per  $^{\circ}\text{F}$  per cubic foot of the packing. The surface area of bed material per cubic foot of tank was determined to be 104 square feet per cubic foot. When the empirical data are used, numerical values of equations (8) and (9) were obtained for various values of  $\tau$  and  $x$ . The resulting values of equation (8) were plotted as functions of their respective values of  $\eta/h$  on a logarithmic scale. The resulting values of equation (9) were plotted as functions of their respective value of  $\xi/h$  also on a logarithmic scale. The construction of these plots did not require the use of the unknown heat-transfer coefficient. These plots were then superimposed on either of the theoretical plots of figure 3. By sliding the  $45^{\circ}$  line on a given experimental plot along the  $45^{\circ}$  line on the correct theoretical plot, a match was made between the experimental curve and one of the family of theoretical curves. When this match was made, the coordinates of the experimental plot were displaced from the coordinates of the theoretical plot by a factor of  $h$ . Therefore, the heat-transfer coefficient was obtained directly. This matching process was performed under the assumption that  $h$  remained constant over a given time and length.

#### DATA PRESENTATION

During this particular program, the pebble-bed heater was operated in a range of airflows between 2.5 pounds per second and 4.9 pounds per second. The blowdown periods ranged between 16 and 46 minutes, while the heating periods (using main burner) ran between 15 and 37 minutes. The maximum outlet air temperature attained was approximately  $2600^{\circ}\text{R}$ . A typical air temperature history encountered during the program is shown in figure 4. The initial temperature rise was typical and was probably due to radiative cooling of the top of the bed and to incomplete combustion within the free volume between the burner and the bed during the heating cycle. An attempt was made to operate the bed well below the maximum design temperature in order to keep the thermocouple instrumentation intact.

A plot of bed temperature against distance from the bottom of the bed is shown in figure 5. The temperatures plotted are those along the vertical axis of the bed. The shape of this profile is similar to all those obtained during the program. The temperature of the lower portion of the bed remained essentially at the temperature achieved through the use of the banking burner alone.

The plot of the bed temperature against radial distance from the center of the bed (fig. 6) indicates that the radial temperature gradient near the centerline at a given level is reasonably flat. Investigation of the radial profiles at other levels in the bed indicates the same result, thus verifying the second assumption made in the theoretical analysis. The sharp increase in temperature at the wall as time progresses is to be expected with the large heat-storage capacity of the insulating brick.

The temperature at a given level in the bed is plotted in figure 7 as a function of blowdown time. Time was measured from the instant the three-way proportioning valve was switched. The shape of this curve is representative of those obtained from the thermocouples in the lower portion of the bed.

Raw data were reduced into usable quantities by substitution into the right sides of equations (8) and (9). The time and distance slopes were obtained from plots such as those shown in figures 5 and 7. Slopes were taken from the time plots at intervals of 2 minutes at various levels in the lower part of the bed. From the distance plots, slopes were taken at intervals of 0.5 of 1 foot at various times during blowdown. Only those thermocouples in the lower portion were used because of the intermittent functioning of the thermocouples near the top of the bed. The center portion, where  $(\partial t / \partial x)_r \approx 0$ , was not usable for the determination of the heat-transfer coefficient.

The value of  $h$  resulting from matching the experimental and theoretical curves for a typical set of data has been substituted into equations (8) and (9), and the resulting points superimposed on the theoretical plots. These are shown in figure 8 and indicate the match between the experimental and theoretical curves.

## RESULTS AND DISCUSSION

### Pressure Drop Data

The pressure drop across the pebble bed was measured and related to the various flow parameters. Since these data were not collected under isothermal flow conditions, it was not possible to compare them directly with those from available references. However, by correcting the observed data for the changes in density due to the nonisothermal flow, the data compare very favorably with those of reference 10. It was not necessary to correct the data for differences in pressure since the bed was operated at a pressure of 1 atmosphere.

### Heat-Transfer Coefficient

Considerable scatter of heat-transfer-coefficient values resulted from the initial application of the analysis. It was found that small temperature differences between that of the inlet gas and that of the bed at a given time and point created unreliable values of the coefficient. This condition existed toward the end of the blowdown periods. By setting a minimum temperature difference of  $100^{\circ}\text{F}$ , some of the doubtful data were eliminated and the amount of scatter was lessened.

The time interval over which the value of the coefficient was determined also had an effect on the amount of scatter. It is evident from figure 8(b) that a small time interval would reduce the length of the experimental curve, thus making the match between it and one of the theoretical curves more arbitrary. Any values obtained during an interval of less than 4 minutes were discarded.

Another cause of scatter was the small distance over which some of the values of the coefficient were obtained. The plots of figures 3(a) and 8(a) show that the use of data obtained over a small distance in the bed would again result in an arbitrary value of the coefficient. It was found that a confident match of data could be made over a distance greater than 1 foot.

A further criterion was used to test the validity of the data. For each match of a pair of experimental and theoretical curves made, two values of the heat-transfer coefficient resulted. One was from the coordinates of the plots, and the other from the parameter  $\eta$  or  $\xi$ . Theoretically, the two values should have been identical. However, in some cases, where the arbitrary condition was not eliminated by the application of the criteria discussed previously, deviations occurred between the two values. A plot was made of the coordinate values of  $h$  against the parametric values of  $h$ . Any values of  $h$  which fell outside a range described by the average relative deviation from a  $45^{\circ}$  line on this plot ( $\pm 28.3$  percent) were omitted.

Table I lists all the reliable values of the coefficient with their respective mass velocities, Reynolds numbers, and Stanton numbers. The specific heat of air which is used in the Stanton number is based on the computed mean film temperature of the air for the time and distance at which the particular value of the coefficient was obtained. The same temperature was used in determining the viscosity of the air which appears in the Reynolds number. The characteristic length used is the average diameter of a pebble, 0.415 inch. The range of Reynolds numbers is from 281 to 771, while for the Stanton numbers it is from 0.022 to 0.073. The value of the coefficient  $h$  ranged between 6.0 and 15.2.

These data are plotted in figure 9 in the conventional form of the  $\text{StPr}^{2/3}$  against  $\text{Re}$ . The Prandtl number for the range of temperatures

investigated is 0.65. A straight line on logarithmic scale was fitted to the data using the method of least squares. The resultant equation is

$$\text{StPr}^{2/3} = 0.400 \text{ Re}^{-0.437} \quad (10)$$

From a statistical viewpoint, the data have a standard deviation of 25.2 percent with a near normal distribution.

Figure 9 shows the order of magnitude in which these data fall in relation to those of other investigators. The upper curve is a composite of the results of references 11 to 13 on packed beds of spheres and represents the order of magnitude generally found in the literature. The intermediate curves represent the data of Dabora, et al. (ref. 1) for alumina balls and of Johnson (ref. 8) for wire screens. They agree reasonably well with the present work. The lowest curve represents the design curve for the facility (ref. 4).

### CONCLUSION

Heat-transfer coefficients have been obtained by transient measurements in a large pebble-bed heater under the conditions specified by the theoretical analysis. The results are recommended for the design of similar facilities. The heat-transfer data obtained in reasonably sized beds, such as that used in reference 1, tend to support this conclusion.

Lewis Research Center

National Aeronautics and Space Administration

Cleveland, Ohio, November 13, 1959

### REFERENCES

1. Dabora, E. K., et al.: Description and Experimental Results of Two Regenerative Heat Exchangers. 2284-18-T, Eng. Res. Inst., Univ. Mich., Feb. 1958. (Contract AF 18(600)-1199.)
2. Bloom, Martin H.: A High Temperature-Pressure Air Heater (Suitable for Intermittent Hypersonic Wind-Tunnel Operation. TN 55-694, WADC, Nov. 1956.
3. Liu, Tung-Sheng, Sun, Ernst J. C., and Knutson, Robert K.: Construction of a Wind Tunnel Simulating the Aerodynamic Heating Effects of Aircraft Structures. TR 56-215, WADC, May 1956.
4. Norton, C. L., Jr.: Pebble Heater - A New Heat Transfer Unit for Industry. Chem. and Metall. Eng., vol. 53, no. 7, July 1946, pp. 116-119.

5. Misteli, John A.: An Investigation of the Corrosion of Alumel Wire in a Swaged MgO Thermocouple Sheath. B. G. Corp., Ridgefield (N.J.), Jan. 1957.
6. Staff of the Lewis Laboratory: Central Automatic Data Processing System. NACA TN 4212, 1958.
7. Glawe, George E., Simmons, Frederick S., and Stickney, Truman M.: Radiation and Recovery Corrections and Time Constants of Several Chromel-Alumel Thermocouple Probes in High-Temperature, High-Velocity Gas Streams. NACA TN 3766, 1956.
8. Johnson, J. E.: Regenerator Heat Exchangers for Gas-Turbines. R. & M. 2630, British ARC, 1952.
9. Schumann, T. E. W.: Heat Transfer: A Liquid Flowing Through a Porous Prism. Jour. Franklin Inst., vol. 208, 1929, pp. 405-416.
10. Anon.: Calculating Pressure Drop Through Packed Beds of Spheres and 1/4 Inch to 8 Mesh Granular Material. Aluminum Co. Am., Pitts. (Pa.), Aug. 24, 1956.
11. Gamson, B. W., Thodos, G., and Hougen, O. A.: Heat, Mass and Momentum Transfer in Flow of Gases Through Granular Solids. Trans. Am. Inst. Chem. Eng., vol. 39, no. 1, Feb. 25, 1943, pp. 1-32; discussion, pp. 32-35.
12. Denton, W. H., Robinson, C. H., and Tibbs, R. S.: The Heat Transfer and Pressure Loss in Fluid Flow Through Randomly Packed Spheres, I. HPC-35, British AERE, 1949.
13. Coppage, J. E.: Heat Transfer and Flow Friction Characteristics of Porous Media. Tech. Rep. 16, Dept. Mech. Eng., Stanford Univ., Dec. 1, 1952. (Contract N6ONR-251.)

TABLE I. - TABULATION OF HEAT-TRANSFER DATA

Mass velocity, G, lb $\frac{1}{(\text{hr})(\text{sq ft})}$	Heat-transfer coefficient, h, Btu $\frac{1}{(\text{hr})(^\circ\text{F})(\text{sq ft})}$	Reynolds number	Stanton number
722	14.5	281	0.073
722	7.6	371	.041
854	6.0	372	.026
854	7.9	375	.036
998	11.6	398	.042
998	8.6	515	.034
1058	11.1	447	.040
1105	10.2	547	.036
1105	8.7	542	.030
1105	11.0	592	.039
1175	7.6	612	.025
1175	9.2	475	.028
1280	7.0	537	.033
1280	15.2	718	.047
1280	12.3	657	.037
1280	9.5	771	.030
1285	12.4	447	.036
1285	12.6	654	.038
1352	10.8	633	.030
1382	8.4	589	.022

E-724

CC-2 back

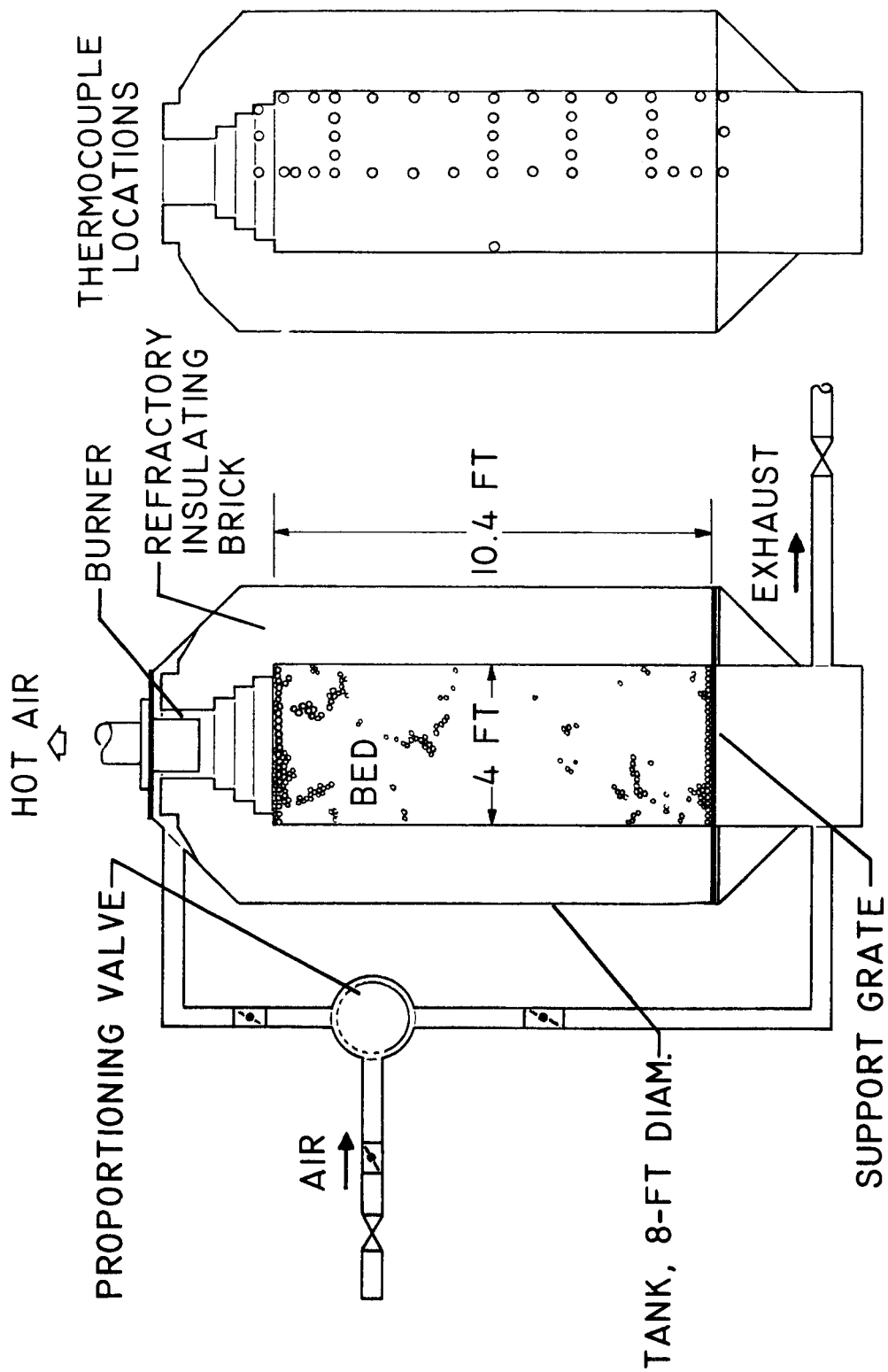


Figure 1. - Pebble-bed facility.

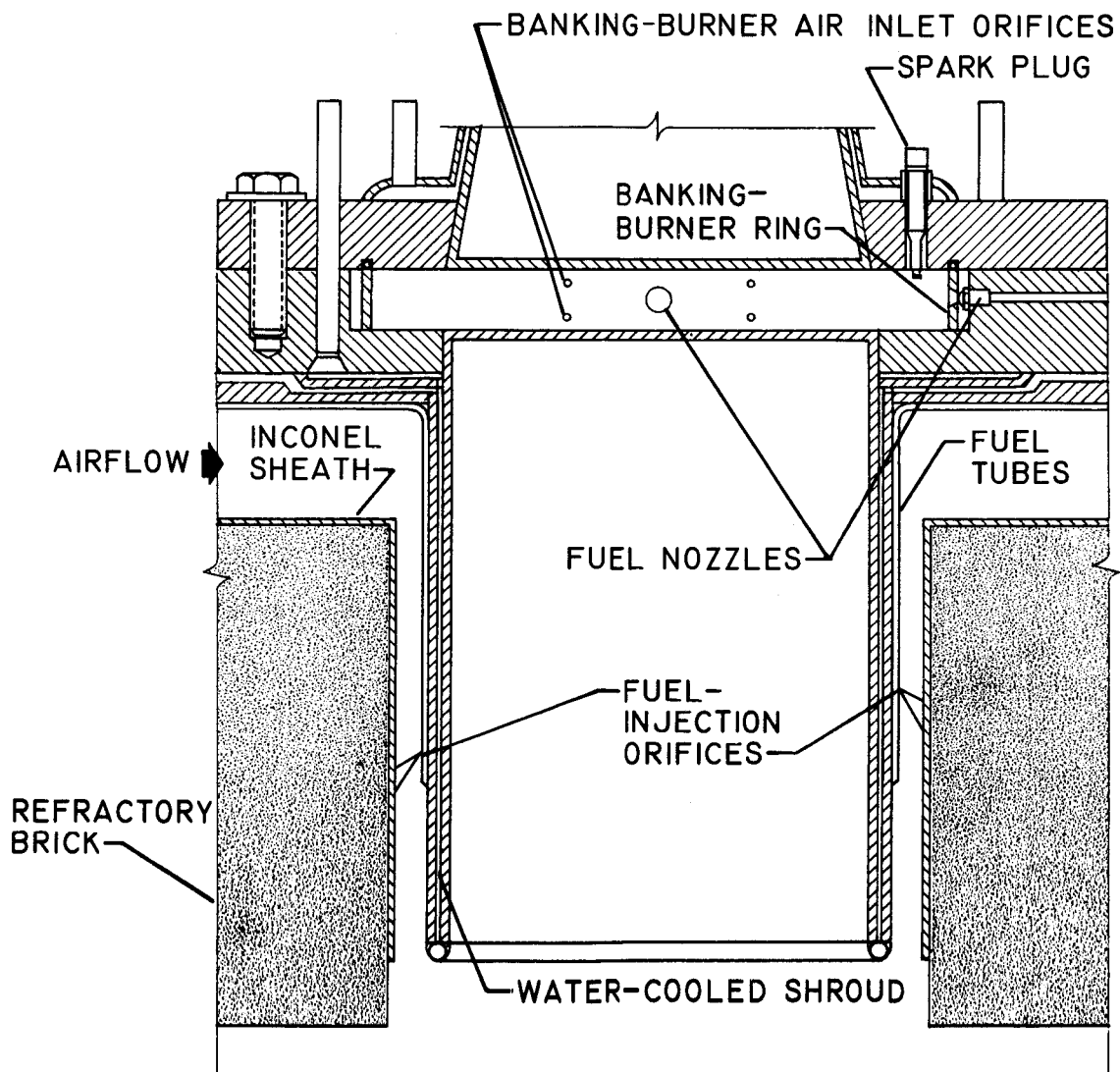
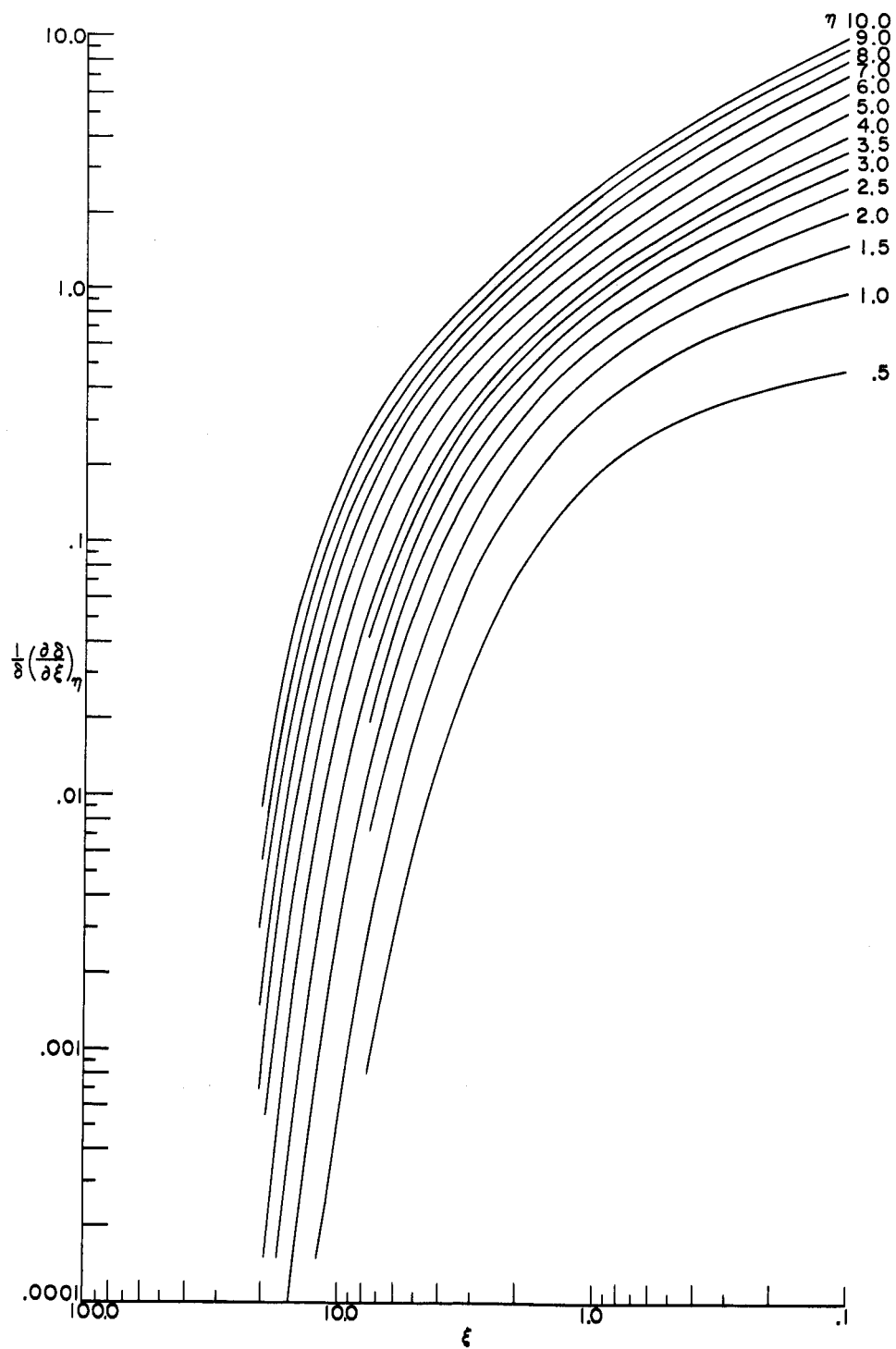
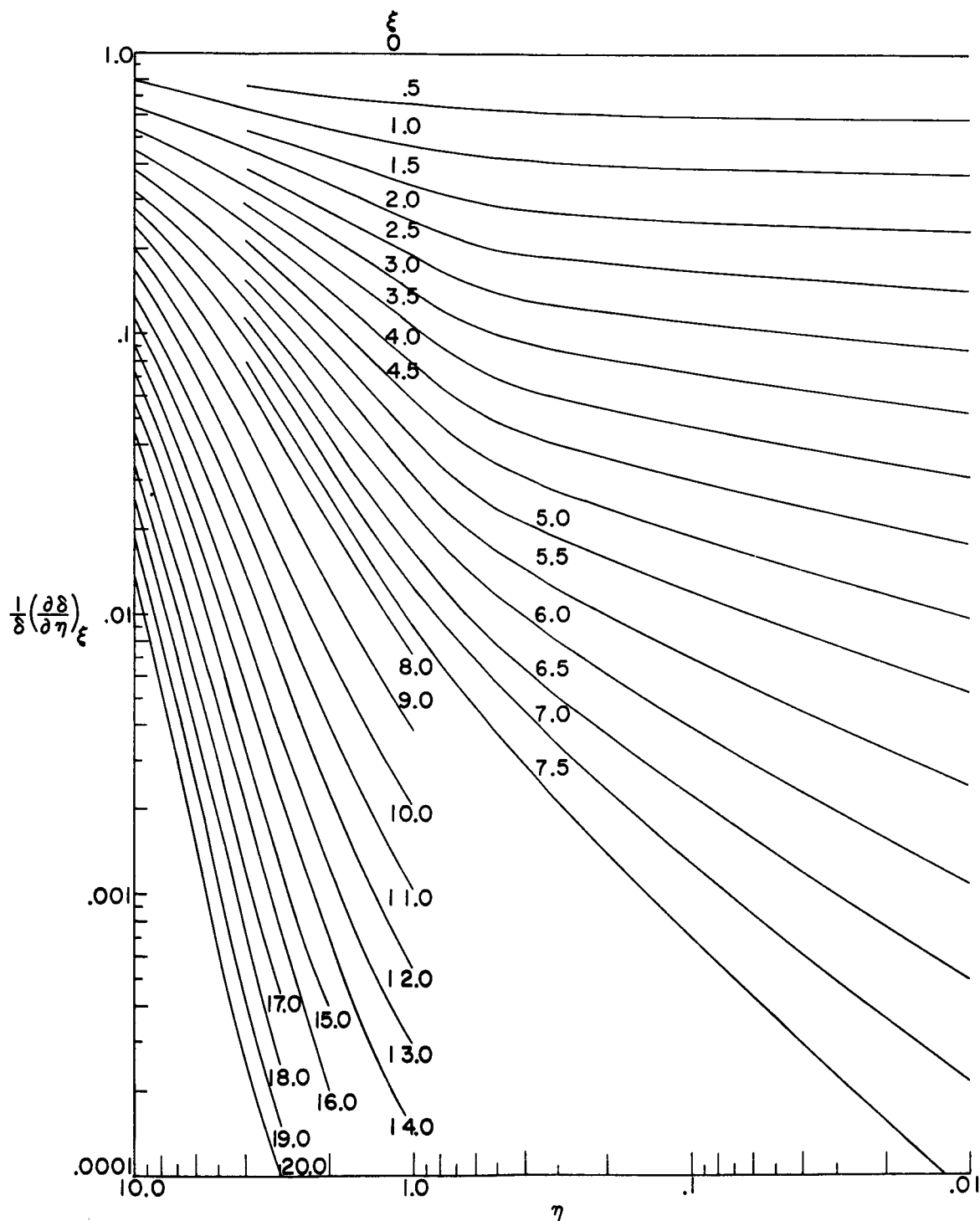


Figure 2. - Banking and main burners.



(a) Bed temperature slope plotted against distance at various times.

Figure 3. - Theoretical plots of nondimensional bed temperature data against various parameters.



(b) Bed temperature slope plotted against time at various distances.

Figure 3. - Concluded. Theoretical plots of nondimensional bed temperature data against various parameters.

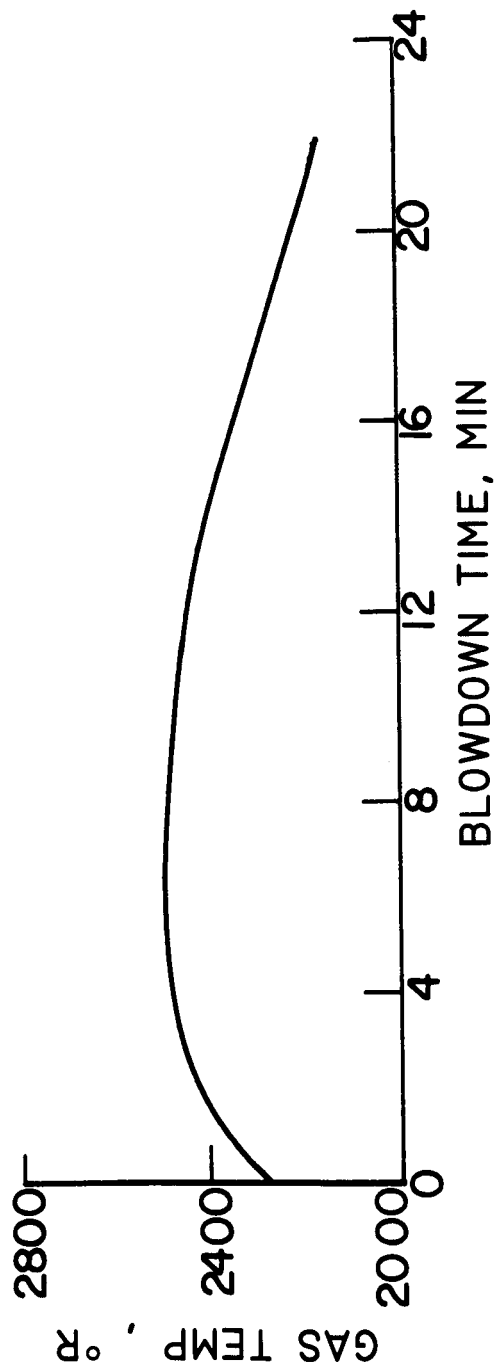


Figure 4. - Air-exit-temperature history as measured with platinum - platinum-rhodium aspirated thermocouple probe. Mass velocity, 717 pounds per hour per square foot.

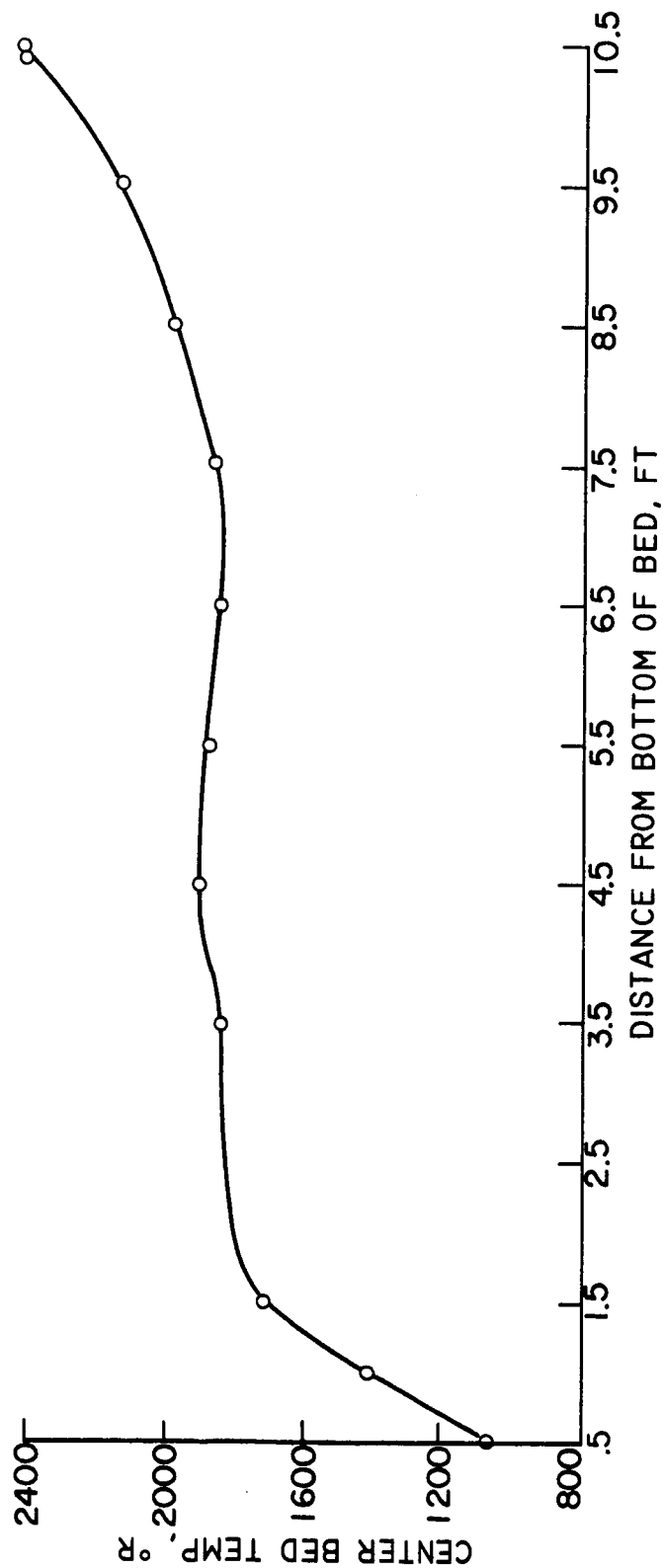


Figure 5. - Bed temperature profile 1 minute after beginning of blowdown period. Mass velocity, 717 pounds per hour per square foot.

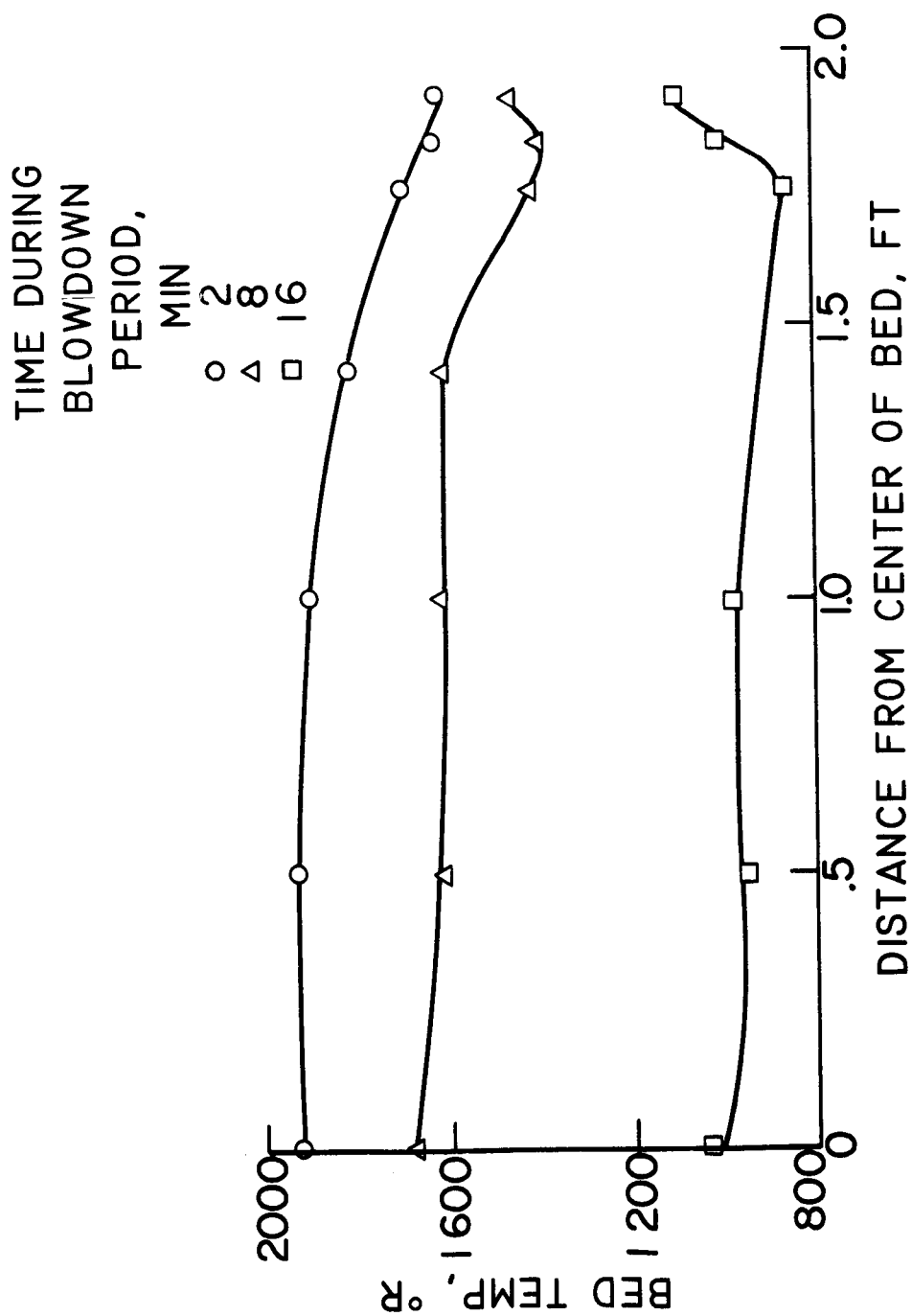


Figure 6. - Bed temperature radial profile 1.5 feet from bottom at several times during blowdown period.

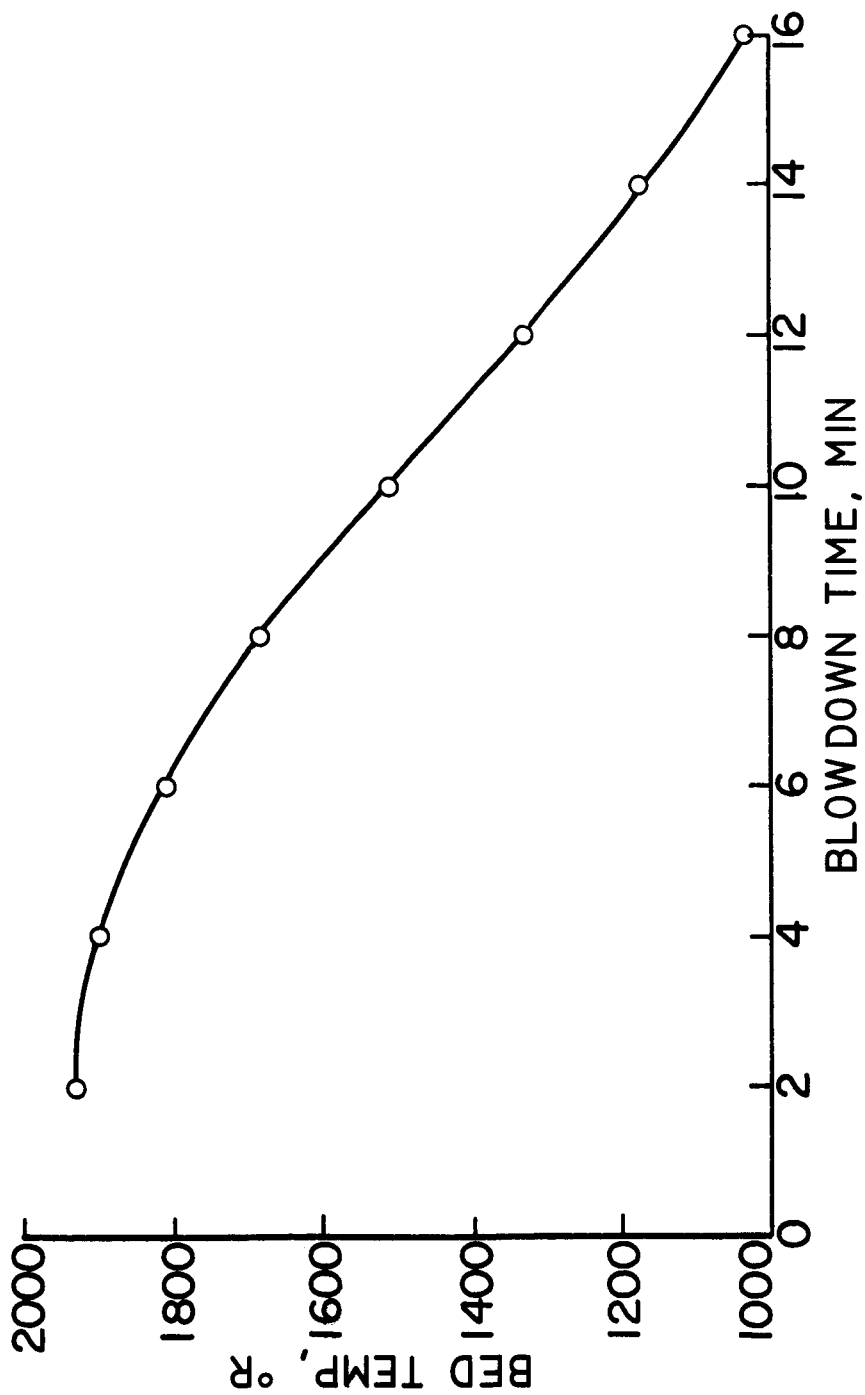
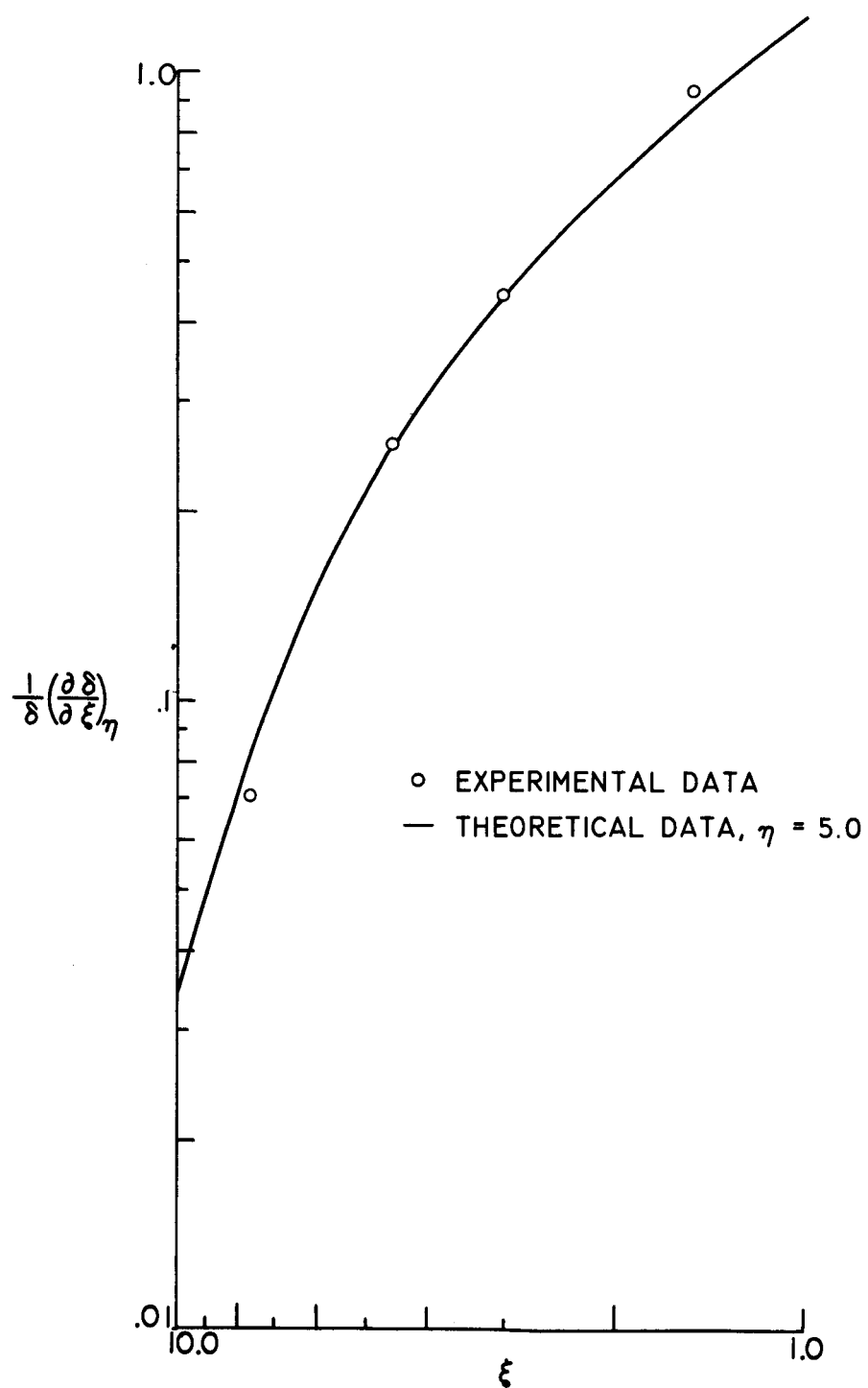
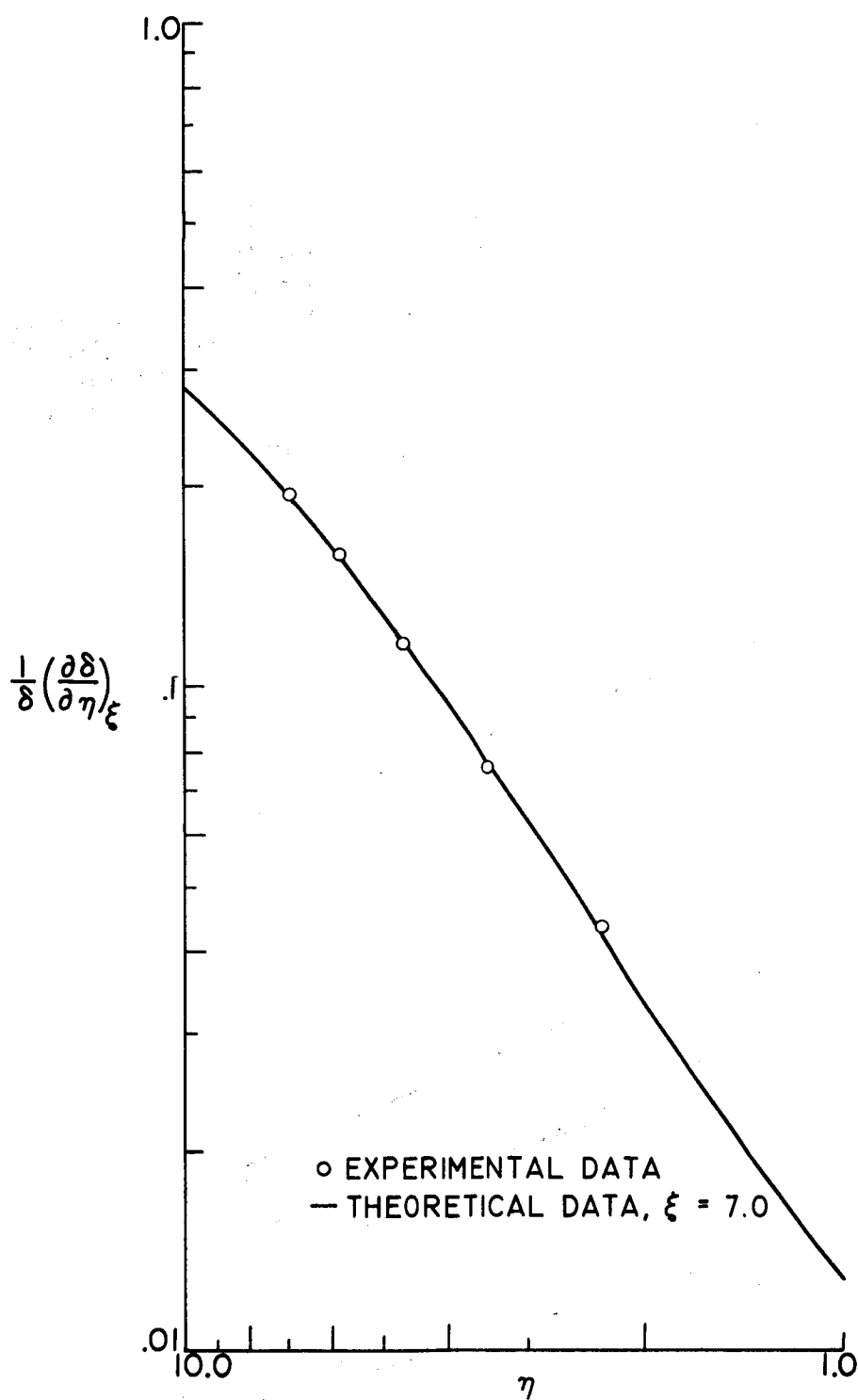


Figure 7. - Bed temperature history 1.5 feet from bottom. Mass velocity, 1058 pounds per hour per square foot.



(a) Nondimensional bed temperature slope plotted against nondimensional distance.

Figure 8. - Comparison of experimental and theoretical data.



(b) Nondimensional bed temperature slope plotted against nondimensional time.

Figure 8. - Concluded. Comparison of experimental and theoretical data.

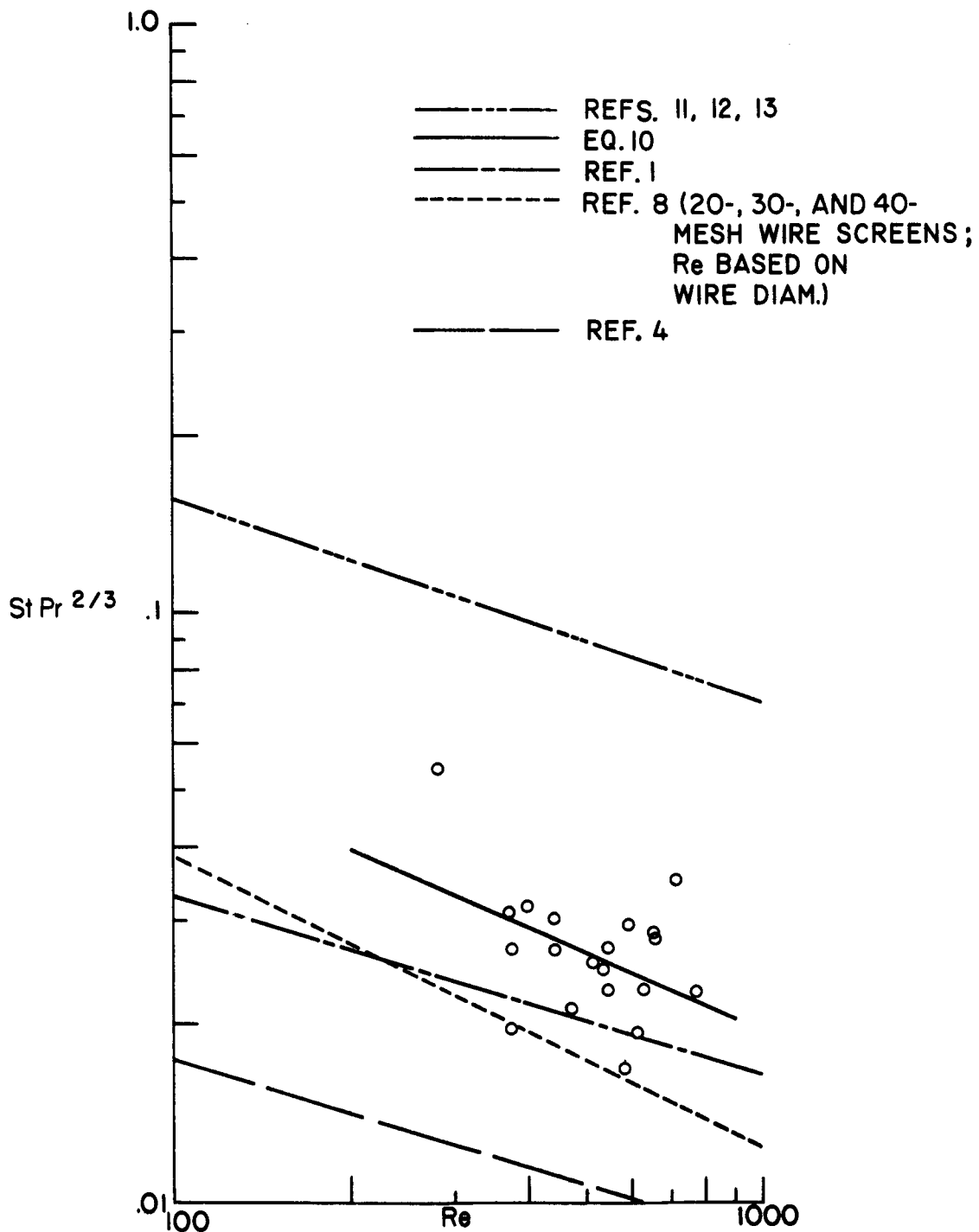


Figure 9. - Correlation of heat-transfer data.